Acta Cryst. (1998). D**54**, 558–569

Structure of Holo-glyceraldehyde-3-phosphate Dehydrogenase from *Palinurus versicolor* Refined at 2 Å Resolution

Shiying Song, Jun Li and Zhengjiong Lin*

National Laboratory of Biomacromolecules, Institute of Biophysics, Beijing 100101, China.
E-mail: lin@nlblinzj.ibp.ac.cn

(*Received 27 May 1997; accepted 10 November 1997*)

Abstract

The crystal structure of holo-glyceraldehyde-3-phosphate dehydrogenase from *Palinurus versicolor*, South China sea lobster, was determined and refined at 2 Å resolution to an *R* factor of 17.1% and reasonable stereochemistry. The structure refinement has not altered the overall structure of GAPDH from this lobster species. However, some local changes in conformation and the inclusion of ordered solvent model have resulted in a substantial improvement in the accuracy of the structure. Structure analysis reveals that the two subunits including NAD^+ in the asymmetric unit are remarkably similar. The thermal differences between the two subunits found in some regions of the NAD^+-binding domain may originate from different crystallographic environments rather than from an inherent molecular asymmetry. In this structure, the side chain of Arg194 does not point toward the active site but forms an ion pair with Asp293 from a neighboring subunit. Structural comparisons with other GAPDH's of known structure reveal that obvious contrast exists between mesophilic and thermophilic GAPDH mainly in the catalytic domain with significant conformational differences in the S-loop, β7-strand and loop 120–125; the *P*-axis interface is more conserved than the *R*- and *Q*-axis interfaces and the catalytic domain is more conserved than the NAD^+-binding domain. Some possible factors affecting the thermostability of this enzyme are tentatively analyzed by comparison with the highly refined structures of thermophilic enzymes.

1. Introduction

D-Glyceraldehyde-3-phosphate dehydrogenase (E.C. 1.2.1.12) is an important enzyme in both glycolysis and glyconeogenesis. It catalyzes the oxidative phosphorylation of D-glyceraldehyde-3-phosphate to form 1,3-diphosphoglycerate in the presence of NAD^+ and inorganic phosphate. The enzyme, consisting of four identical subunits, is allosteric and shows a variety of cooperative properties. GAPDH structures were first determined for the enzymes from lobster (*Homarus americanus*) muscle, and then for that from the moderate thermophile *Bacillus stearothermophilus* in several conformational states (Moras *et al.*, 1975; Murthy *et al.*, 1980; Skarzynski *et al.*, 1987; Skarzynski & Wonacott, 1988). In addition, there are several crystallographic investigations for enzymes from other species such as human muscle (Mercer *et al.*, 1976), *Bacillus coagulans* (Griffith *et al.*, 1983), *Trypanosoma brucei* (Vellieux *et al.*, 1993), *Thermotoga maritima* (Korndorfer *et al.*, 1995), *Thermus aquaticus* (Tanner *et al.*, 1996), and *E. coli* (Duée *et al.*, 1996). These structural investigations provide important information on the folding, catalysis, allosterism mechanism, as well as the thermal stability of this important enzyme.

The interesting half-of-the-sites properties of the enzyme when reacting with certain chemical modification reagents (Levitzki, 1974) has been related to its allosteric function. The well studied reaction leading to the formation of NAD^+ fluorescent derivative by irradiation of carboxymethylated GAPDH† (Ho & Tsou, 1979), is also half-of-the-sites for the muscle and yeast enzymes. Structural studies of native carboxymethylated and irradiated GAPDH will further contribute to our knowledge of its catalytic and allosteric mechanisms. We have previously reported results of crystallographic studies of GAPDH from South China Sea lobster *Palinurus versicolor* including crystallization (Song *et al.*, 1983), molecular replacement (Gao *et al.*, 1988) and the 2.7 Å structure of irradiated GAPDH (Lin *et al.*, 1993). During these studies it became clear that detailed analysis of the structure and mechanism requires a high-resolution refined structure. This paper presents the refined structure of PV holo-GAPDH at 2.0 Å resolution. The refinement at this resolution permitted an accurate description of the three-dimensional structure including solvent molecules, thus could serve as an accurate reference structure for future analyses of carboxymethylated and irradiated GAPDH. In addition, the refinement could help to resolve the question

† Abbreviations used: GAPDH, D-glyceraldehyde-3-phosphate dehydrogenase; BS, *Bacillus stearothermophilus*; HA, *Homarus americanus*; PV, *Palinurus versicolor*; TM, *Thermotoga maritima*; TA, *Thermus aquaticus*; EC, *Escherichia coli*; r.m.s., root-mean-square, G (green), R (red), B (blue) and Y (yellow) stand for the individual subunits of the tetramer (following the naming scheme for the HA structure).

concerning possible minor molecular asymmetry of lobster GAPDH by comparison of the subunit structure, and to delineate more precisely the conserved and variable parts of the structure of the GAPDH molecule, and to analyze the factors affecting the enzyme's thermostability by comparison with the well refined structures of *Bacillus stearothermophilus* and other thermophilic GAPDH's.

2. Experimental methods

2.1. *Crystallization, data collection and processing*

The enzyme was purified from the tail muscle of South China Sea lobster, *Palinurus versicolor*, essentially according to the method of Allison & Kaplan (Allison & Kaplan, 1964). The crystals were grown by vapour diffusion over $(NH_4)_2SO_4$ and have space group of $C2$ with cell dimensions $a = 128.40$, $b = 99.90$ and $c = 80.79$ Å and $\beta = 114.48^\circ$ with only half of the molecule in each asymmetric unit (Song *et al.*, 1983). The crystals diffract to at least 2.0 Å and are very stable during exposure to synchrotron radiation at low temperature.

The data set was collected at the BL6A2 station of the KEK photon factory in Japan with a synchrotron radiation imaging-plate Weissenberg camera system (Sakabe, 1983) at a temperature of 7°. The rotation axis of $a + b$ and a short wavelength of 1.00 Å were used to reduce the absorption error. The rotation range covered 0–202°. The data were then processed by the *WEIS* program (Higashi, 1989). The data set has an $R_{\rm merge}$ of 0.069 including 84 900 independent reflections to 1.7 Å resolution, and an $R_{\rm merge}$ of 0.250 in the resolution range 2.03–2.11 Å. The data redundancy are 1.6 and 1.2 for all data and for the last shell, respectively.

2.2. *Starting model*

The structure of PV GAPDH carrying a fluorescent derivative (Irr-GAPDH) was solved previously (Lin *et al.*, 1993) at 2.7 Å resolution by molecular replacement and then refined by the least-squares method assuming the sequence is identical to that of *Homarus americanus*. This structural determination provided a water-free model that was used as the starting model for a high-resolution structure analysis of holo-GAPDH, which crystallized in the same crystal form as Irr-GAPDH. Before refinement, the rotation function was checked again using the *GLRF* program (Liang & Rossmann, 1990). The result gave the same peak as reported previously (Lin *et al.*, 1993) but showed that it was more prominent than determined previously, indicating the correctness of the structure solution. The result of the *GLRF* calculation is described briefly here. The self-rotation calculations using data between 10 and 5 Å and an integration radius of 30 Å yielded a unique peak (10.5σ) at $\varphi = 25$, $\psi = 90$ and $\chi = 180^\circ$. This peak together with a crystallographic twofold axis was interpreted as resulting from 222 point symmetry. Cross-rotation function calculations using the 2.9 Å model of the HA GAPDH tetramer and data between 10 and 6 Å with a space group of $P2_1$ and an integration radius of 50 Å yielded a unique peak (18.6σ) at $\varphi = 90$, $\psi = 25$ and $\chi = 90^\circ$ (maximum background is 5.14σ). This peak clearly identifies the absolute orientation of the tetramer, *i.e.* the molecular Q axis is parallel to the b axis, the P axis is parallel to the a axis and the R axis is parallel to the c^* axis. The molecular origin was fixed to the crystallographic twofold axis b by the space group.

2.3. *Crystallographic refinement*

In view of the small percentage of the data completeness in the outer shell (2.0–1.7 Å), only 2 Å data were used in the refinement, which contains 49 184 unique reflections with $F > 3\sigma$, corresponding to a completeness of 81.64% between 6 and 2 Å, and a completeness of 46.53% for the last shell (2.00–2.09 Å). The structure was refined in several steps by a combination of positional refinement and simulated annealing with the program *X-PLOR* (Brünger, 1992). Standard *X-PLOR* topology and parameter files were employed in the refinement of the protein and the coenzyme NAD^+. For detecting the possible differences between the two subunits in the asymmetric unit, refinement was carried out by treating each subunit independently without imposing non-crystallographic twofold symmetry restraints on the subunits. During the refinement, several manual adjustments were made on an SGI workstation using the program *TURBO* with the $2F_o - F_c$ electron-density map or $F_o - F_c$ electron-density map. Large adjustments were made on the conformation of NAD^+ in the green subunit and in segments 189–195, 275–280, 297–302, 22–29 *etc*. Water molecules were gradually included in the model. They were positioned only when well defined positive peaks existed in both the $2F_o - F_c$ and $F_o - F_c$ difference maps and when they could form hydrogen bonds either with protein atoms or other water molecules. Sulfate ions were identified by their bulk density. Inconsistencies between the model and the electron density were found for a few side chains, indicating possible sequence differences between PV and HA GAPDH. These residues were corrected based on the electron-density distribution in both subunits as well as in carboxymethylated GAPDH (unpublished results).

3. Results and discussion

3.1. *Model quality*

The final model containing 5012 non-H protein atoms, two NAD^+ molecules, four sulfate ions and 366 solvent water molecules for the red and green subunits gives an R factor of 17.1% for reflections with $F>3\sigma$ and 18.0% if including all weak reflections in the resolution range

6.0–2.0 Å. The R_{free} factor was calculated to be 22.3% for 11.2% reflections with $F>3\sigma$ in the same resolution range. The model has stereochemistry with r.m.s. deviations of 0.014 Å for bond lengths, 2.85° for bond angles and 25.92° for torsion angles.

The main-chain and side-chain atoms have well defined corresponding electron densities except for several segments. The segments lacking well defined densities (electron-density correlation coefficients less than 0.7) include 1–2, 60–61, 69–92, 98–117, 134–143, 329–334 in the *R* subunit and the two C-terminal residues in the *G* subunit. Most of these are located on the surface of the molecule and exposed to the solvent. Nevertheless, the structure of these segments could be recognized and determined although not as accurately as for other parts. The distributions of main-chain dihedral angles (φ, ψ) for the green and red subunits are shown on the Ramachandran plot (Ramachandran *et al.*, 1963) in Fig. 1. All non-glycine residues are within the allowed regions except residues Ala147, Val237 and Glu166. These three residues have well defined electron densities. The unfavorable dihedral angles of these residues have been observed in other GAPDH structures (Skarzynski *et al.*, 1987; Duée *et al.*, 1996).

A Luzzati plot suggests that a lower bound for the coordinate error is about 0.22 Å (Luzzati, 1952). Least-squares superposition of C_α atoms belonging to the red and green subunits gives an r.m.s. separation of less than 0.20 Å (see below). These values are comparable to those found for protein structures of similar resolution.

The average *B* factor is 32.4 Å^2 for all protein atoms; the average *B* factors for the catalytic and coenzyme-binding domains are 21 and 29 Å^2 in the green subunit, and 24 and 53 Å^2 in the red subunit. The higher average *B* factor for the coenzyme-binding domain as compared with that of the catalytic domain has been observed previously (Tanner *et al.*, 1996), and this structure shows more obvious differences of the *B* factors between the two domains. The *B* factors averaged over the main chain for the two subunits are plotted in Fig. 2 as functions of residue number.

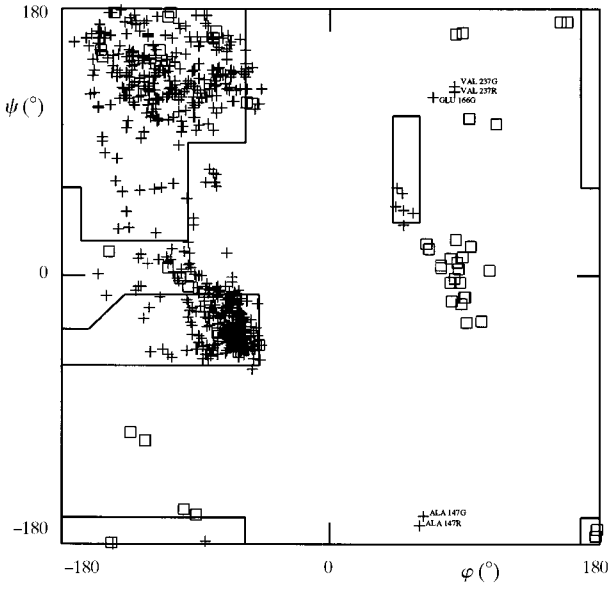

Fig. 1. Ramachandran plot (Ramachandran *et al.*, 1963) of the distributions of main-chain dihedral angles (φ, ψ) for the green and red subunits.

3.2. *Effect of refinement*

Refinement of the PV GAPDH model has not altered the overall structure reported earlier (Lin *et al.*, 1993). However, some local conformational changes and the inclusion of the ordered solvent molecules resulted in substantial improvements in the accuracy of the structure. During the refinement, the backbone conformations of several segments were substantially modified. These include segments 1 (189–195), 2 (275–280), 3 (297–302) and 4 (22–29) in both subunits and the NAD^+ molecule in the green. Fig. 3 shows three of these regions in the final model together with the final electron density. The first three segments are involved in intersubunit interactions, thus understanding their conformations is an important part of understanding the structure and function of this enzyme. The side-chain orientations of some residues such as Arg194, Trp193 and Trp310 were also significantly modified.

3.3. *Sequence correction*

Sequence differences between the PV and HA GAPDH were revealed from the present study. Residue 270, a Phe in the HA sequence, is replaced by a Val on the basis of the small electron density extending from the Cα atom, and the valine at this position frequently occurs in other GAPDH's, Asp6, Asp236 and Ile284 are replaced by a Asn, Asn and Thr, respectively, as a result of the close contact of their side-chain atoms with neighboring residues, and the replacements result in formation of hydrogen bonds (Asp6 ND2···Glu94 OE1; Asp236 ND2···312Asp OD1, OD2; and Thr284 OG1 ···Cys281 O). Sequence correction includes (with the residue for the HA sequence in parentheses) Glu21(Ser), Ala59(Met), Ile117(Val), Lys142(Thr), Ala261(Thr), Ile325(Leu), *etc.* There are 13 differences altogether. Although the replacements appear to be

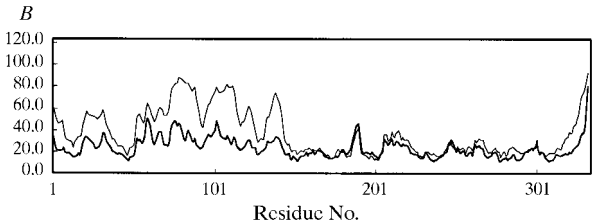

Fig. 2. Temperature-factor variation *versus* residue number for the main chains in the green subunit (thick line) and the red subunit.

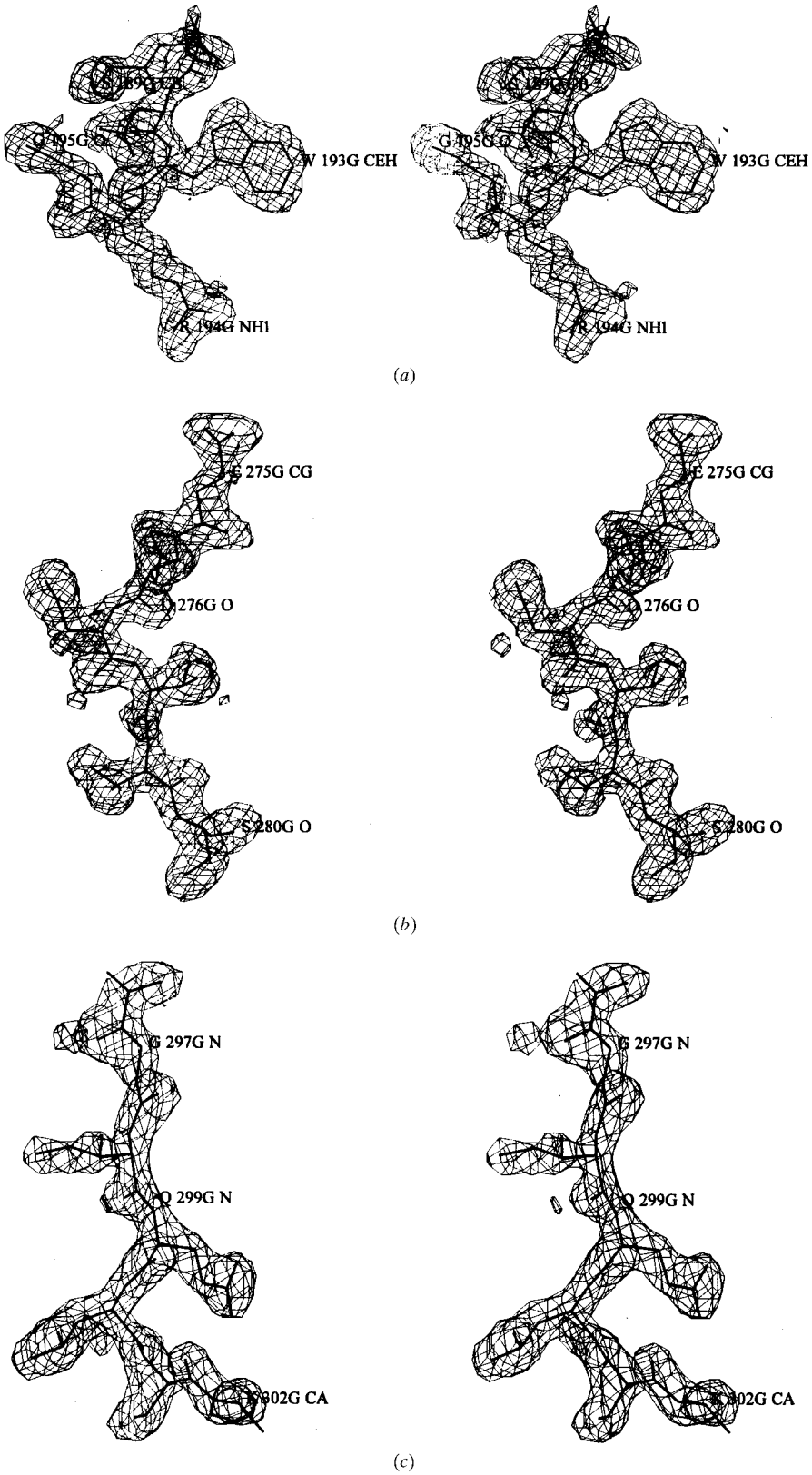

Fig. 3. Peptide segments with large adjustments along with the corresponding electron densities in the final electron-density map: (*a*) segment 189–197, (*b*) segment 275–280 and (*c*) segment 297–302. Data are shown for the green subunit only.

Table 1. *R.m.s.d. (Å) of Cα atomic positions between PV GAPDH and other GAPDH's*

The data were taken from entry 1GD1 for BS (Skarzynski *et al.*, 1987), entry 1HDG for TM (Korndorfer *et al.*, 1995), entry 1CER for TA (Tanner *et al.*, 1996) and entry 1GAD for EC (Duée *et al.*, 1996) in the Protein Data Bank. The numbers in the brackets indicate the sequence identity. The green subunit of PV, the P subunit of EC and the R subunits of BS, TA and TM were used for the domain and subunit calculations. In these calculations, the sequences were aligned in accord with those in PDB. All deletions/insertions were left out of the superposition except that for residues 22 and 23 in TM instead of 18a and 18b were deleted, and residue 125 in BS, TA and TM instead of 122a was deleted.

	EC	BS	TA	TM
NAD^+-binding domain	0.894 (53%)	0.963 (50%)	1.100 (46%)	1.219 (44%)
Catalytic domain	0.329 (79%)	0.606 (57%)	0.683 (53%)	0.785 (53%)
Subunit	0.686 (66%)	0.822 (54%)	0.988 (49%)	1.120 (48%)
Dimer (*R* axis)	0.915	1.032	1.102	1.437
Dimer (*Q* axis)	0.781	1.048	1.066	1.369
Dimer (*P* axis)	0.743	0.901	1.039	1.168
Tetramer	0.844	1.243	1.118	1.551

evident from the structure at this resolution, direct determination of the sequence is still needed for final conformation.

3.4. *Overall structure*

The enzyme is a tetramer consisting of four identical subunits designated as the green (G), red (R), blue (B) and yellow (Y) subunits and having three molecular axes designated as *P*, *Q* and *R*, following the nomenclature of HA structure. In the *C*2 crystal, the molecular *Q* axis is a strict crystallographic twofold axis and the molecular *R* axis has no significant deviations from true twofold axis as calculated by the transformations from red to green subunits ($\kappa = 179.63^\circ$, $t = 0.12$ Å). Thus, the tetramer shows good 222 symmetry. Each subunit consists of two domains: the catalytic domains (148–311) and the NAD^+-binding domains (1–147 and 312–333). The high-resolution structure reveals much detail which could not be seen clearly at medium resolution. For examples, the *S*-shaped loop (178–201) is well defined, consists of a short piece of 3_{10} helix (192–197), three β-turns (179–182, 189–192 and 198–201) and two main-chain hydrogen bonds (Lys183 O···Ala199 N, Gly187 N···Gly197 O); Helices αD and αF consist of two and three 3_{10} helices, respectively. In the following description and discussion, only subunit *G* will be analyzed and compared with the other GAPDH's except for in §3.8. Fig. 4 (Kraulis, 1991) shows the general folding of a subunit including the secondary-structure elements which are designated in accordance with the nomenclature adopted for BS (Biesecker *et al.*, 1977) and EC (Duée *et al.*, 1996). The figure was produced using *MOLSCRIPT* (Kraulis, 1991). As can be seen from Fig. 3, the overall subunit structure is very similar to those from other GAPDH's.

For structure comparison, four GAPDH structures with resolutions higher than 2.5 Å in the Protein Data Bank were used. They are BS (entry 1GD1; Skarzynski *et al.*, 1987), TM (entry 1HDG; Korndorfer *et al.*, 1995), TA (entry 1CER; Tanner *et al.*, 1996), and EC (entry 1GAD; Duée *et al.*, 1996). Of these, EC is mesophilic and the rest are thermophilic. The r.m.s. deviations of the Cα atomic positions between PV and other GAPDH's were calculated after least-squares superposition. The data are listed in Table 1 together with the sequence homology. In these calculations, all deletions/insertions were left out of the superposition (see the

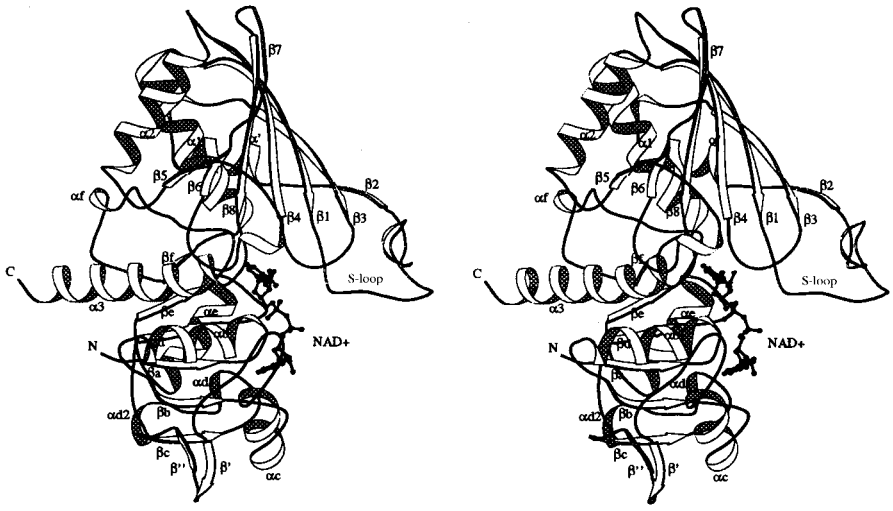

Fig. 4. Ribbon diagram of PV GAPDH subunit structure. The coenzyme NAD^+ is indicated. (Figure produced using *MOLSCRIPT*; Kraulis, 1991.)

legend of Table 1 for details). The results show the well conserved structural features despite the low sequence homology with the thermophilic enzymes (the maximum Cα r.m.s. deviation for a tetramer is only 1.551 Å), and remarkable structural similarity between the two highly homologous mesophilic enzymes especially in the catalytic domain (the corresponding value is only 0.329 Å, much less than the values ranging from 0.606 to 0.785 Å between PV and the thermophilic enzymes). The Cα r.m.s. deviations also show that in each case the catalytic domain had a greater structural conservation compared with the NAD^+-binding domain and in each case involved in the thermophilic enzymes, the *P*-axis related dimer had a greater structural conservation compared with the other dimers. These structural features correspond well with the sequence identity.

Fig. 5 shows the subunit Cα backbone structure of PV superimposed onto BS, revealing some local differences. Cα r.m.s. deviations for PV and BS are plotted along the polypeptide chain in Fig. 6. Which yields eight peaks (>2 Å) in the regions near residues 23, 34, 61, 86, 123 and 139 of the NAD^+-binding domain and residues 190 and 297 of the catalytic domain. The plots for TA and TM (data not shown) are similar except for additional peaks near 248 (in TA) and 209 (in TM) and missing peaks near 86 (in TA) and 139 (in TM). We next briefly describe the structure differences in these regions.

3.4.1. *Loop 23–26*. This is an extended loop connecting αB to βB. The conformational differences here come from the insertion of residue 24 in BS, and the insertions of 18a, 18b and 24 in TM. The insertions make the loop protrude outward and become exposed to the solvent environment.

3.4.2. *Loop 33–35*. This connects βB to αC. PV has a proline inserted at 34, which is absent in other structures. This insertion in PV makes the loop protrude outward, so that the bulky hydrophobic side chains of Pro33 and Phe34 can stay at a position in which to interact with the adenine moiety of NAD^+.

3.4.3. *Turn 60–63*. This turn connects two β-strands which are located on the outer side of the β-sheet in the NAD^+-binding domain. The turn seems to lack interactions with neighboring segments, thus being flexible and having high *B* factor in each structures.

3.4.4. αD_2 *84–88*. The conformational difference in this portion comes from the replacement of Ala89 in PV by Val with a larger side chain than in the other GAPDH's. The side chain of this residue is in contact with the neighboring strand βA of the β-sheet.

3.4.5. *Loop 120–125*. This loop connects two β-strands, βE and β. In all three thermophilic structures, the loop forms three main-chain hydrogen bonds with neighboring loops, *i.e.* 122 N···100 O, 122 O···102 N and 125 N···143 O. In BS and TM, a salt bridge between Asp125 and Arg102 is present. But all these interactions are missing in PV. This may weaken the connection between different structural elements connecting with the β-sheet in the NAD^+-binding domain in PV (Fig. 7). The high *B* factor in this region (Fig. 2) provides additional support for the inference.

3.4.6. *Turn 138–141*. This is a β-turn with 138 O···141 N hydrogen bond. In BS and TA, because of the insertion of 138a, one turn of α-helix forms there. TM is similar to PV as it has a deletion at this area.

3.4.7. *S-loop (178–201)*. In PV, an additional β-turn (189–192) forms in this portion because of the insertion of Ser189. This extra turn interacts with *R*-axis related subunit, thus creating some differences in the intersubunit interaction pattern of the *R*-axis interface (see below). Moreover, in the *S*-loop region of thermophilic enzymes, four charged residues Asp181, Arg183, His190 and Arg195 form a series of salt bridges or hydrogen bonds, which connects different segments within the *S*-loop. They include Asp181 O···His190 NE2,

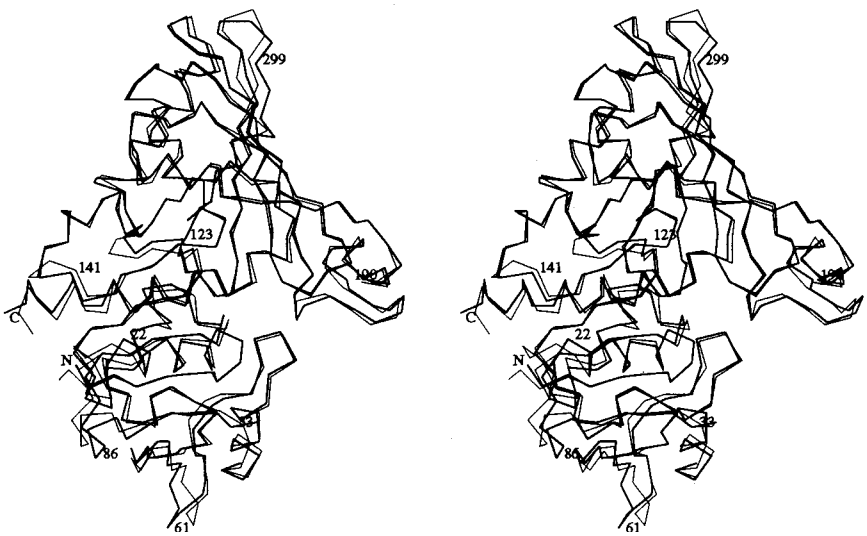

Fig. 5. Cα backbone of a subunit of PV GAPDH superimposed onto the BS GAPDH (thick line represents the green subunit of PV GAPDH, thin line represents the red subunit of BS GAPDH).

Asp181 OD1···His190 NE2, Arg183 NE···Pro188 O, Arg183 NH2···Pro188 O and Asp181 OD1···Arg195 NH1, *etc.* While these interactions do not exist in PV due to the changes of the turn conformation and the loop sequence (Fig. 8*a* and Fig. 7*b*). The absence of these interactions may weaken the connection between the different segments within the *S*-loop. The high *B* factors in this region (Fig. 2) support this inference.

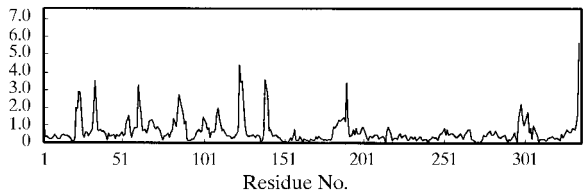

Fig. 6. Cα r.m.s. differences between PV GAPDH (the green subunit) and BS GAPDH (the red subunit) along the polypeptide chain.

3.4.8. *β7-strand (298–301)*. This is an extensively refined region. β7, the external strand of β-sheet in the catalytic domain, constitutes a part of *P*-axis related interface. The conformation of β7-strand is modified due to the replacement of Tyr252 from the neighboring loop in PV by Val or Ala in thermophilic GAPDH's, as the side chain of this residue is in contact with the strand. This conformational difference does not disrupt the hydrogen-bonding pattern of β7 with neighboring strand β8. However, the connection between β7 and β8 differs

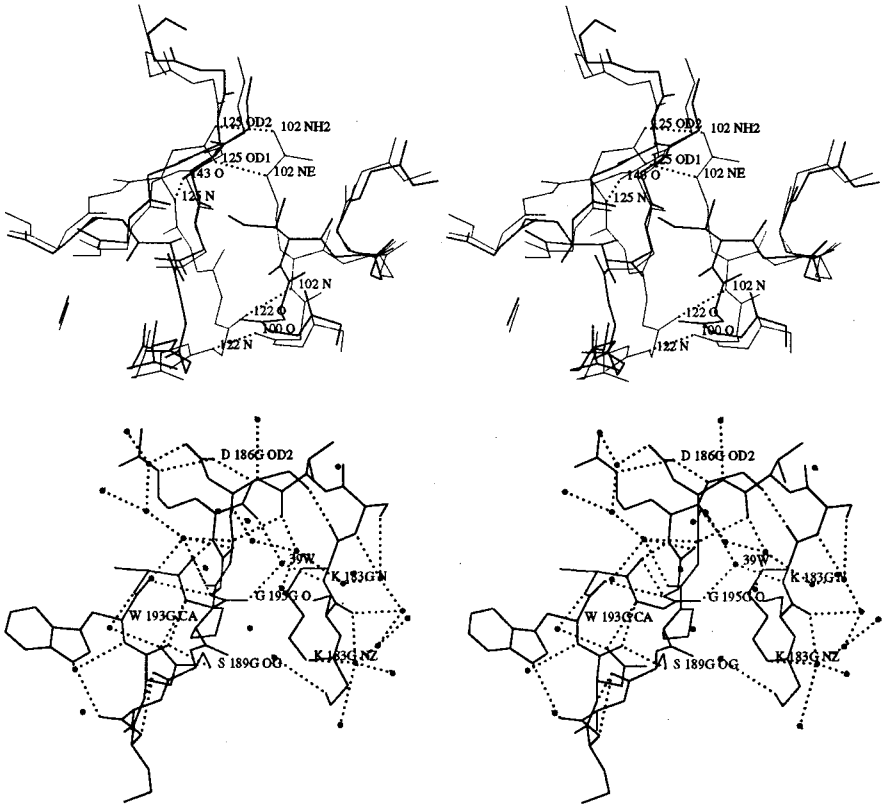

Fig. 7. Difference between loop 120–125 region of PV GAPDH (thick line, the green subunit) and BS GAPDH (thin line, the red subunit). The loop 120–125 in BS is stabilized by some main-chain hydrogen bonds and a salt bridge.

Fig. 8. Difference between the *S*-loop region of (*a*) the green subunit of PV GAPDH and (*b*) the red subunit of BS GAPDH. In BS, some main-chain hydrogen bonds and salt bridges connect different segments within the *S*-loop which are absent in PV.

significantly. In PV, a type I turn with hydrogen bond 301 O to 304 N occurs at the location, while in BS, a type I′ turn with bifurcated hydrogen bonds 300 O to 303 N and 204 N links β7 and β8. Nevertheless, the main-chain hydrogen bond connecting the turn to the loop, *i.e.* 250 N···302 O, remains unchanged in all structures.

As described above, both difference regions in the catalytic domain may be important for function. Of the six difference regions in the NAD^+-binding domain, loop 33–35 forms in part the adenine-binding subsite and loop 120–125 is related to the stability of the β-sheet, which in turn may affect the binding of NAD^+. The remaining four are located on the side opposite to the NAD^+-binding site, thus may have less effect to the function of the enzyme.

The plot of Cα r.m.s. deviation for EC (data not shown) is very plain without significant peaks in the catalytic domain, indicating the remarkable conformational similarity between the two mesophilic enzymes in this area. Thus, the conformational differences in the *S*-loop and β7-strand observed above may be closely related to the functional differences between the mesophilic and thermophilic enzymes, especially the *S*-loop to the thermostability. In contrast with the catalytic domain, the plot in the NAD^+-binding domain shows similar characteristics as that for BS. That is because many peaks in this domain are in the sequence variable (insertion/deletion, or specific replacement) area for both mesophilic and thermophilic enzymes. Therefore, the conformational differences in the NAD^+-binding domain may not be related to the thermostability except loop 120–125, where most of interactions which occur in thermophilic but are missing in PV as mentioned above do not exist in EC either, but they may be related to the thermostability.

3.5. *NAD^+ site and active site*

The electron density of the NAD^+ molecules is well defined in both green and red subunits. Their geometry and interactions with the protein molecule are extremely similar in both subunits. As in the red subunit, the adenine ring in the green subunit is roughly perpendicular to the planes of the neighboring ribose with an *anti* conformation. The conformational parameters of NAD^+ shows the remarkable similarity to that of BS GAPDH. The maximum differences in the dihedral angles for NAD^+ are ξa and ξn (19° for the *G* subunit). The interactions of NAD^+ with the protein include seven direct hydrogen bonds and a similar number of water-mediated hydrogen bonds. All the direct and most of the indirect hydrogen bonds are identical to those of BS. The hydrogen bond NAD^+—OP2A···Asn180 ND2 in BS is absent in this structure with the replacement of Asn180 by Ala. Compared with BS, the residues forming direct interaction with the adenine moiety are more hydrophobic. Leu33, Thr34, Arg77 and Arg98 in BS are replaced by Pro, Phe, Met and Val, respectively. Of which, Pro33 and Phe34 are common to other muscle GAPDH. This structure reveals that the prolyl ring of Pro33 and the phenol ring of Phe34 point to the adenine ring, resulting in strong hydrophobic interaction as shown in Fig. 9. These hydrophobic side chains may help define the orientation of the adenine moiety. However, like other GAPDH structures, the direct hydrogen bond NAD^+—N6A···Arg77 O and the water-mediated hydrogen bonds NAD^+—N1A···Wat O···Asn6 ND2 and Glu76 O remain unchanged.

The catalytically important residues Cys149 and His176 and the suggested phosphate-binding residues Thr179, Arg231, Ser148 and Thr208 are located in the lowest r.m.s. deviation region (Fig. 6). The superposition of all atoms from these residues gives an r.m.s. deviation of 0.339 Å for PV and BS, indicating that the site is extremely similar. As in BS, the ND atom of His176 is also hydrogen bonded to the carbonyl O atom of Ser177, thus playing a role in fixing the plane of the histidine imidazole ring. The location of the sulfate ions which identify the attacking inorganic phosphate ion P_i and the substrate phosphate ion P_s and their interaction with protein atoms, also closely resemble to those of BS except that the distance between P_i and Cys149 SG is slightly shorter (6.41 and 6.37 Å in G and R subunits, respectively) and the electron-density peak of P_i elongates to face Cys149 SG. This structure feature implies multi-position occupancy, which is consistent with the

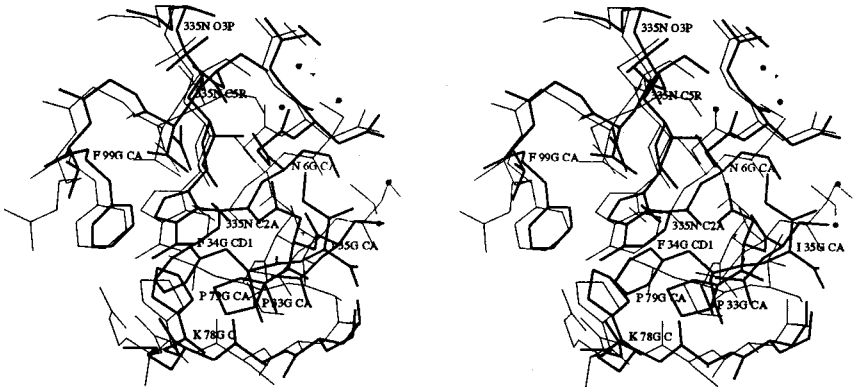

Fig. 9. Difference between the adenine subsite of PV GAPDH (thick line; the green subunit) and BS GAPDH (thin line; the red subunit). PV has more hydrophobic character in this subsite.

previously reported BS model study (Skarzynski *et al.*, 1987), showing the possibility of moving the P_i anion towards the S atom of Cys149 by about 1.5 Å without any significant change in the number and type of interactions. It was found that Arg194 does not point toward the active site but forms an ion pair with Asp293 from a neighboring subunit (see below). Thus, it is impossible for the residue to take part in the formation of the inorganic phosphate site during catalysis structurally equivalent to Arg195 in BS (Skarzynski *et al.*, 1987).

3.6. *Subunit interfaces*

The subunit interfaces in PV were analyzed with respect to their hydrogen-bonding pattern including salt bridges. All the intersubunit interactions with a difference cut-off of 3.4 Å are listed in Table 2. Extensive interactions exist at the interfaces between *P*-axis related subunits and between *R*-axis related subunits with only a few interactions belonging to the *Q*-axis related subunits. All the interactions in PV are identical to EC, implying that the interaction pattern may be common to mesophilic enzymes. However, there exist some differences from the thermophilic enzymes.

In PV, extensive interactions exist on the *R*-axis interface in the contact region between the *S*-loop of the catalytic domain and the helix αC and the following turn (47–51) of the NAD^+-binding domain from the neighboring subunit. Thermophilic enzymes contain fewer polar interactions in this region. As compensation they have more hydrophobic interactions. In PV, Trp193, Tyr39 and Tyr42 form aromatic–aromatic interactions and hydrogen bonds involving the phenolic hydroxyl groups of the two tyrosines. The presence of the intersubunit aromatic cluster in PV may lead to a small translational movement of the subunit from the center of the molecule relative to those of other enzymes. In other muscle GAPDH's, a similar situation may exist as these residues are conserved for these enzymes. The ordered-water structure on this interface is partially different from that of BS.

The *P*-axis related subunits involve 20 interactions of which most are identical to thermophilic enzymes. These interactions mainly involve the antiparallel β-sheet, α-helix 280–284 and the *S*-loop of the catalytic domain. It is to be noted that the extensive refinement of the *S*-loop results in the close-up of the guanidino group of Arg194 to the carboxyl group of Asp293 in the *P*-axis related subunit, forming an ion pair Arg194–Asp293 similar to that in other GAPDH's. This ion pair is not unique in thermophiles but also exists in PV and therefore, is not responsible for the thermostability, contrary to the previous suggestions (Walker *et al.*, 1980). Among the known structures, the BS may have the most intersubunit ion pairs, but not all are important for structure and thermostability. For example, the intersubunit ion pair Arg169–Glu245 exists in BS, but not in TM and TA due to the sequence difference. In PV, although these two residues are replaced by residues with opposite charge, so it would be possible to form an ion pair. But in fact they form an intrasubunit rather than an intersubunit ion pair.

The data indicate that the *P*-axis related interactions are conserved more than the *R*-axis related interactions. This result is consistent with the lower Cα r.m.s. deviations for the *P*-axis dimer than the other dimers (Table 1). This inference agrees with that reached from BS GAPDH structure (Biesecker *et al.*, 1977). Thus, together with the observation that the interactions in the *P*-axis interface are stronger than those in the *R*-axis and the *Q*-axis, the arrangement of four subunits can be

Table 2. *Intersubunit hydrogen bonds and salt bridges*

Residue 1	Residue 2	Distances (Å)	Angles (°)
G···R			
OEH Tyr39G	N Ser189R	2.70	175.9
N Ser189G	OEH Tyr39R	2.65	158.0
OEH Tyr42G	NH2 Arg197R	3.16	165.5
NH1 Arg197G	OEH Tyr42R	3.07	160.1
N Ser48G	OD1 Asp186R†	3.02	174.4
OD1 Asp186G	N Ser48R†	2.96	175.1
OG Ser48G	OD2 Asp186R†	2.67	142.9
OD2 Asp186G	OG Ser48R†	2.56	141.8
OG Ser48G	NH1 Arg197R†	3.08	136.2
NH1 Arg197G	OG Ser48R†	3.25	133.9
OG Ser48G	ND2 Asn202R‡	3.11	158.2
ND2 Asn202G	OG Ser48R‡	3.05	160.3
OG1 Thr49G	NE2 Gln201R	2.84	143.7
NE2 Gln201G	OG1 Thr49R	3.07	164.6
O Thr179G	OG1 Thr184R	2.89	154.9
OG1 Thr184G	O Thr179R	2.83	121.9
G···B			
OEH Tyr42G	O Asp277B	2.69	141.3
O Asp277G	OEH Tyr42B	2.69	141.3
OEH Tyr46G	OD1 Asp276B‡	2.85	150.5
OD1 Asp276G	OEH Tyr46B‡	2.85	150.5
G···Y			
OG1 Thr173G	OD1 Asp241Y†	2.64	147.4
OD1 Asp241G	OG1 Thr173Y†	2.78	152.8
OG1 Thr173G	NZ Lys306Y‡	3.01	135.7
NZ Lys306G	OG1 Thr173Y‡	2.92	133.2
NH1 Arg194G	OD1 Asp293Y†	2.80	157.6
OD1 Asp293G	NH1 Arg194Y†	2.83	157.1
NH2 Arg194G	OD2 Asp293Y†	3.01	168.6
OD2 Asp293G	NH2 Arg194Y†	3.01	170.5
NH1 Arg194G	O Val278Y†	2.89	134.9
O Val278G	NH1 Arg194Y†	2.69	136.3
NH1 Arg197G	OD1 Asp282Y†	2.85	171.3
OD1 Asp282G	NH1 Arg197Y†	2.79	166.9
NH2 Arg197G	OD2 Asp282Y†	2.89	149.8
OD2 Asp282G	NH2 Arg197Y†	2.94	154.6
N Ile203G	OG Ser280Y‡	2.88	171.1
OG Ser280G	N Ile203Y‡	2.90	153.2
O Ile203G	N Ser280Y†	3.05	159.1
N Ser280G	O Ile203Y†	3.14	167.7
OD1 Asn202G	N Ser281Y‡	2.82	162.8
N Ser281G	OD1 Asn202Y‡	2.88	161.9

† Identical to BS, TA, TM. ‡ Identical among two out of three thermophilic enzymes.

regarded as consisting of two *P*-axis related dimers (red and blue, yellow and green).

The number of hydrophobic interactions in the subunit interfaces were estimated by the calculation of accessible surface area of hydrophobic residues buried in the tetramer using the program *CCP*4. The values are 6373 (PV), 6016 (EC), 7312 (BS), 7461 (TA) and 7289 (TM). The general trend of increased hydrophobic interactions from mesophilic to thermophilic are evident in agreement with the view presented by other authors (Korndorfer *et al.*, 1995; Tanner *et al.*, 1996).

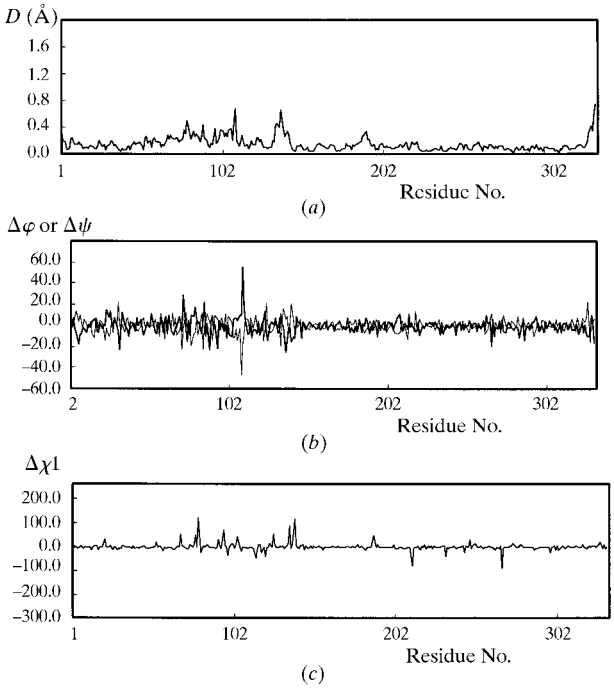

Fig. 10. (*a*) A variation of the average positional differences for the main-chain atoms between the green and red subunits *versus* residue number. (*b*) A variation of $\Delta\varphi$ and $\Delta\psi$, the dihedral angle differences for the main-chain atoms between the green and red subunits, *versus* residue number (thick line, $\Delta\varphi$, thin line, $\Delta\psi$). (*c*) A variation of $\Delta\chi1$, the dihedral angle difference for the side-chain atoms between the green and the red subunits, *versus* residue number.

3.7. *Similarity of subunit structure*

The r.m.s. deviation of the atomic positions calculated after a least-squares superposition of the two subunits in the asymmetric unit was 0.199 Å for the Cα atoms and 0.220 Å for the main-chain atoms. The catalytic domain shows higher similarity (0.116 Å for the main-chain atoms). Fig. 10(*a*) gives the positional differences between the green and red subunit along the chain for the main-chain atoms. Some slight differences (greater than 0.4 Å) were observed in the NAD^+-binding domain, particularly in residues 79–80, 89, 108–109, 134–138 and 330–333. These regions have less well defined electron density in the red subunit. Segment 330–333 is the C-terminal end of the polypeptide chain. The other regions have a different crystallographic environment for the two subunits: in the red subunit they are on the surface exposed to the surrounding solvent, while in the green subunit the corresponding regions are in contact with the similar region of the blue subunit from a neighboring molecule (Lin *et al.*, 1993). Therefore, these differences may not be of significance.

The main-chain dihedral angle differences, $\Delta\varphi$ and $\Delta\psi$, along the chain showed similar patterns (Fig. 10*b*). From the pattern fewer spikes were observed compared with the plot of positional differences, indicating greater conservation of the secondary structure between the two subunits. The largest spike in both plots corresponds to residues 111 at the C-terminal of helix *E*, which is situated in a different crystallographic environment for the two subunits.

The r.m.s. deviations for all non-H protein atoms including those of the side chains are 0.396 Å for the catalytic domain and 0.517 Å for the NAD^+-binding domains. The mean difference of the dihedral angle $\chi1$ for all the side chains between the green and the red subunits is only 8.9°. This small value of $\Delta\chi1$ shows that the structural similarity between the two subunits could be extended to include most of the side chains. A residue-by-residue comparison of $\Delta\chi1$ (Fig. 10*c*) shows fewer spikes. Most of these spikes concentrate in the NAD^+-binding region from residues 69 to 139, similar to

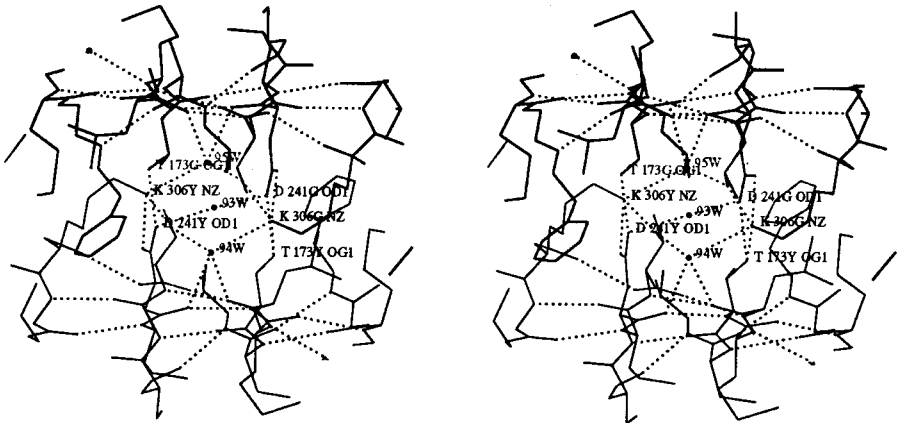

Fig. 11. Ordered water molecules with non-crystallographic symmetry in the region around the molecular *P* axis.

the patterns of Figs. 10(*a*) and 10(*b*), except for the two extra spikes corresponding to Lys212 and Gln268 in the catalytic domain. Among the spikes six have larger $\Delta\chi1(>70^\circ)$ and eight more are included if the difference is larger than 40°. Interestingly, seven of these are lysine and four are proline. These $\chi1$ differences obviously arise from the conformational flexibility, lysine has long side chain and the Cγ atom of proline can occupy alternative positions. No significant side-chain asymmetry was found which results from the close intersubunit contact except for Pro233. The active site and all the aromatic residues show excellent symmetry.

The catalytic domains in the two subunits have comparable *B* factors and the same variation pattern along the chain. However, the *B*-factor pattern for the NAD^+-binding domains for the two subunits differ with some residues in the red subunit having significantly higher *B* factors than those in the green subunit (Fig. 2). This thermal difference pattern correlated well with the small positional difference pattern. The NAD^+-binding domain of the green subunit is well fixed due to the numerous lattice contacts giving a low *B* factor, while that of the red subunit lacks close lattice contacts and, therefore, is less ordered or more mobile giving a higher *B* factor.

In the asymmetric unit there are a total of 366 ordered water molecules of which 102 pairs occupy non-crystallographic equivalent positions with an equivalence cut-off of 1.0 Å. Fig. 11 shows the non-crystallographic symmetry of the ordered-water structure in the region around the molecular *P* axis.

In solution, lobster muscle GAPDH exhibits negative cooperativity in coenzyme binding (De Vijlder *et al.*, 1969; Zhao *et al.*, 1985), a phenomenon which could be explained on the basis of two models: ligand-induced asymmetry from an *a priori* symmetrical molecule and pre-existing asymmetry (Stallcup & Koshland, 1973; Bernhard & MacQuarrie, 1973). Previous lobster GAPDH structures determined at medium resolution did not provide firm evidence of molecular symmetry. There could be minor structural differences between *R*-axis related subunits in unrefined HA GAPDH structure (Moras *et al.*, 1975). However, some later structural studies such as GAPDH complexed with nicotinamide 8-bromoadenosine dinucleotide, GAPDH with sulfate ions replaced by citrate ions, and apo-GAPDH seem to support the view of molecular symmetry (Olsen *et al.*, 1976*a*,*b*; Murthy *et al.*, 1980). The current high-resolution structure of holo-GAPDH from lobster species PV reveals that the red and green subunits including the two coenzyme molecules in the asymmetric unit are remarkably similar. Thermal asymmetry observed seems to be induced by the lattice forces. It would be interesting to see whether the molecular symmetry observed in NAD^+-saturated GAPDH is maintained in the absence of NAD^+. The structure analysis of apo-GAPDH from the same source is in progress.

4. Conclusions

The structure of PV GAPDH has been refined at 2 Å resolution. The refined structure has not altered the overall structure reported for GAPDH from *Palinurus versicolor* at medium resolution. However, some local conformational changes and inclusion of ordered solvent molecules result in a substantial improvement in the structural accuracy. The new model permits a more precise description of the enzyme and coenzyme structures as well as the solvent structure. The two subunits in the asymmetric unit could be compared with high accuracy.

The information on molecular symmetry is important for understanding the allosteric mechanism of GAPDH. This high-resolution structure reveals that the subunits of the holoenzyme are remarkably similar with no apparent inherent asymmetry for the lobster species *Palinurus versicolor*.

Preliminary structure comparison has been made between PV GAPDH and the other GAPDH's with known structures. Structure comparison shows that the well conserved structural features exist in all enzymes despite the low sequence homology with the thermophilic enzymes; the catalytic domain is more conserved than the NAD^+-binding domain and the *P*-axis interface is more conserved than the other two. Thus, the arrangement of four subunits can be regarded as consisting of two *P*-axis related dimers (red and blue, yellow and green). Structure comparison also shows the obvious contrast between mesophilic and thermophilic GAPDH especially in the catalytic domain with significant conformational differences in the *S*-loop and β7-strand.

The intersubunit ion pair Arg194–Asp293 also exists in the PV GAPDH structure, indicating that this intersubunit salt bridge is not responsible for the thermal stability of the *Thermophilus* GAPDH. The general trend of increased hydrophobic interactions at the subunit interfaces from mesophilic to thermophilic enzymes can be inferred from the accessible surface area of hydrophobic residues buried in the tetramer. On the other hand, the importance of intrasubunit salt bridges and hydrogen bonds for GAPDH thermostability, as analyzed in the *S*-loop and 120–125 loop, regions are emphasized. These observation and analysis support the view presented by other authors (Korndorfer *et al.*, 1995; Tanner *et al.*, 1996).

The coordinate and structure factor data have been deposited in the Brookhaven Protein Data Bank.†

† Atomic coordinates and structure factors have been deposited with the Protein Data Bank, Brookhaven National Laboratory (Reference: 1SZJ and R1SZJSF). Free copies may be obtained through the Managing Editor, International Union of Crystallography, 5 Abbey Square, Chester CH1 2HU, England (Reference: GR0761). At the request of the authors the structure factors will remain privileged until 4 February 2001.

We thank Professor Chenlu Tsou for his most valuable suggestions and discussion during the course of this work and Professor M. G. Rossmann for his most helpful suggestions and discussion in the structure determination and for providing the program *GLRF*. Thanks also go to Professor N. Sakabe for his help in synchrotron data collection. This work was supported by China Natural Science Foundation (grant No. 39 370 164).

References

Allison, W. S. & Kaplan, N. O. (1964). *J. Biol. Chem.* **239**, 2140–2152.

Bernhard, S. A. & MacQuarrie, R. A. (1973). *J. Mol. Biol.* **74**, 73–78.

Biesecker, G., Harris, J. I., Thierry, J. C., Walker, J. E. & Wonacott, A. J. (1977). *Nature (London)*, **266**, 328–333.

Brünger, A. T. (1992). *X-PLOR Manual Version 3.0*, Yale University, New Haven, Connecticut, USA.

De Vijlder, J. J. M., Boers, W. & Slater, E. C. (1969). *Biochim. Biophys. Acta*, **191**, 214–220.

Duée, E., Olivier-Deyris, L., Fanchon, E., Corbier, C., Branlant, G. & Dideberg, O. (1996). *J. Mol. Biol.* **257**, 814–833.

Gao, Y.-G., Song, S.-Y., Li, J., Zhao, B.-G., Xie, G.-F. & Lin, Z. J. (1988). *Acta Biophys. Sin.* **2**, 243–251.

Griffith, J. P., Lee, B., Murdock, A. L. & Amelunxen, R. E. (1983). *J. Mol. Biol.* **169**, 963–974.

Higashi, T. (1989). *J. Appl. Cryst.* **22**, 9–18.

Ho, Y.-S. & Tsou, C.-L. (1979). *Nature (London)*, **277**, 245–246.

Kraulis, P. J. (1991). *J. Mol. Biol.* **227**, 9–14.

Korndorfer, I., Steipe, B., Huber, R., Tomschy, A. & Jaenicke, R. (1995). *J. Mol. Biol.* **246**, 511–521.

Levitzki, A. (1974). *J. Mol. Biol.* **90**, 451–458.

Liang, T. & Rossmann, M. G. (1990). *Acta Cryst.* A**46**, 783–792.

Lin, Z.-J., Li, J., Zhang, F.-M., Song, S.-Y., Yang, J., Liang, S.-J. & Tsou, C.-L. (1993). *Arch. Biochem. Biophys.* **302**, 161–166.

Luzzati, P. V. (1952). *Acta Cryst.* **5**, 802–810.

Mercer, W. D., Winn, S. I. & Watson, H. C. (1976). *J. Mol. Biol.* **104**, 277–283.

Moras, D., Olsen, K. W., Sabesen, M. N., Buehner, M., Ford, G. C. & Rossmann, M. G. (1975). *J. Biol. Chem.* **250**, 9137–9162.

Murthy, M. R. N., Garavito, R. M., Johnson, J. E. & Rossmann, M. G. (1980). *J. Mol. Biol.* **138**, 859–872.

Olsen, K. W., Garavito, R. M., Sabesan, M. N. & Rossmann, M. G. (1976*a*). *J. Mol. Biol.* **107**, 577–584.

Olsen, K. W., Garavito, R. M., Sabesan, M. N. & Rossmann, M. G. (1976*b*). *J. Mol. Biol.* **107**, 571–576.

Ramachandran, G. N., Ramakrishnan, C. & Sasisekhran, V. (1963). *J. Mol. Biol.* **7**, 95–99.

Sakabe, N. (1983). *J. Appl. Cryst.* **16**, 542–547.

Skarzynski, T., Moody, P. C. E. & Wonacott, A. J. (1987). *J. Mol. Biol.* **193**, 131–187.

Skarzynski, T. & Wonacott, A. J. (1988). *J. Mol. Biol.* **203**, 1097–1118.

Song, S.-Y., Gao, Y.-G., Zhou, J.-M. & Tsou, C.-L. (1983). *J. Mol. Biol.* **171**, 225–228.

Stallcup, W. B. & Koshland, D. E. Jr (1973). *J. Mol. Biol.* **80**, 41–62.

Tanner, J. J., Hecht, R. M. & Krause, K. L. (1996). *Biochemistry*, **35**, 2597–2609.

Vellieux, F. M. D., Hajdu, J., Verlinde, C. L. M. J., Groendijk, H., Read, R. J., Reenhough, T. J. G., Campbell, J. W., Kalk, K. H., Littlechild, J. A., Watson, H. C. & Hol, W. G. J. (1993). *Proc. Natl Acad. Sci. USA*, **90**, 2355–2359.

Walker, J. E., Wonacott, A. J. & Harris, J. I. (1980). *Eur. J. Biochem.* **108**, 581–586.

Zhao, G.-Z., Zhou, J.-M. & Tsou, C.-L. (1985). *Chin. Biochem. J.* **1**, 81–86.